

Liquid Assembly of Floating Nanomaterial Sheets for Transparent Electronics

Zongming Su, Henry S. C. Yu, Xiaosheng Zhang,* Juergen Brugger,* and Haixia Zhang*

A novel pattern strategy of a nanomaterial network that can self-assemble onto prepatterned soft substrate to realize ultra-transparent electronics is presented. The approach detailed is based on the combination of nanomaterials' self-assembly at the water–air interface to form nanomaterial networks and the breakage phenomenon of water–nanomaterial membranes to form designed patterns. With the comprehensive investigation of this phenomenon, nanomaterial networks are manipulated to attach to prepatterned sidewalls. This leads to a remarkable transparency improvement without conductive property decline. Three 1D nanomaterials with various geometries are demonstrated to verify the universal feature of this pattern strategy, including silver nanowire (AgNW), carbon nanotube, and zinc oxide nanowire. Furthermore, sequential layer-by-layer deposition of several 1D nanomaterials has also been demonstrated by using the proposed approach, revealing an attractive potential of multiple-junction transparent electronics. The fabricated micro-grid structure of AgNWs with a line width of 5 μm and pitch of 150 μm has a sheet resistance of 37.88 $\Omega \text{ sq}^{-1}$ and an optical transmittance of 86.06%. This fabrication strategy opens up opportunities for different nanomaterials in many transparent and wearable applications.

1. Introduction

In recent years, transparent electronics have attracted much attention in both academia and industry. Electronic products, such as the touch screen^[1] and solar cells,^[2] have proved its wide application prospects on flat substrates, which motivates

researchers to develop transparent devices on flexible or even stretchable substrates. Indium tin oxide (ITO) is one transparent conductor that is most commonly used.^[3] Its high transmittance (>90%) at low sheet resistances (10 $\Omega \text{ sq}^{-1}$ on glass) is the primary reason for its popularity. However, it is brittle and easily prone to cracking. Conducting polymers^[4] are one long-standing alternative to ITO that offer mechanical flexibility. Their limited conductivity as well as low current carrying capacity, however, restrict their further applications.

ITO and conducting polymers are both intrinsically conductive and transparent. Alternatively, partial removal of deposited conductive and nontransparent material is another strategy for high transparent membranes or devices.^[5] By using chemical or physical removal techniques, such as dry or wet etching, unwanted material is stripped from the substrate to achieve the required high transparency. For example, most liquid metal is removed

for high transparent and stretchable liquid metal circuits.^[6] A membrane with 90% transmittance needs to remove at least 90% nontransparent material for light transmission, which results in significant nonreusable waste.


Recently, the use of percolation networks based on nanomaterials (metal nanoparticles,^[7] nanowires,^[3b,8] carbon nanomaterials^[9]) have gained much attention, because this method not only offers high transparency but also reduces the waste of precious nanomaterials. By adopting loose percolation networks, metal nanowires gain remarkable transparency of more than 95%.^[10] However, with increasing amount of nanowires, the transparency decreases and a tradeoff between transparency and nanowire quantity has to be found.

Both mentioned strategies sacrifice the material quantity for transparency improvement. Besides electrical performance, which is normally the target investigation, other device properties (e.g., mechanical robustness) are also influenced when material quantity is sacrificed. When resistance increases,^[11] the uniformity worsens^[12] and the mechanical stability^[13] suffers with a very loose percolation network. However, this dilemma can be solved by adopting space in the third dimension. The idea makes use of the thickness rather than the 2D area to improve material performance and occupy less 2D space for higher light transmittance. For instance, researchers managed to fabricate 3D metal grid mesh via secondary sputtering for high transparency (85.2%) with low resistance (9.8 $\Omega \text{ sq}^{-1}$).^[14]

Dr. Z. Su, Prof. H. Zhang
National Key Laboratory of Science and Technology
on Micro/Nano Fabrication
Institute of Microelectronics
Peking University
Beijing 100871, China
E-mail: hxzhang@pku.edu.cn

Dr. Z. Su, H. S. C. Yu, Prof. J. Brugger
Microsystems Laboratory
Institute of Microtechnique and Institute of Materials
École Polytechnique Fédérale de Lausanne
1015 Lausanne, Switzerland
E-mail: juergen.brugger@epfl.ch

Prof. X. Zhang
School of Electronic Science and Engineering
University of Electronic Science and Technology of China
Chengdu 611731, China
E-mail: zhangxs@uestc.edu.cn

 The ORCID identification number(s) for the author(s) of this article can be found under <https://doi.org/10.1002/admt.201900398>.

DOI: 10.1002/admt.201900398

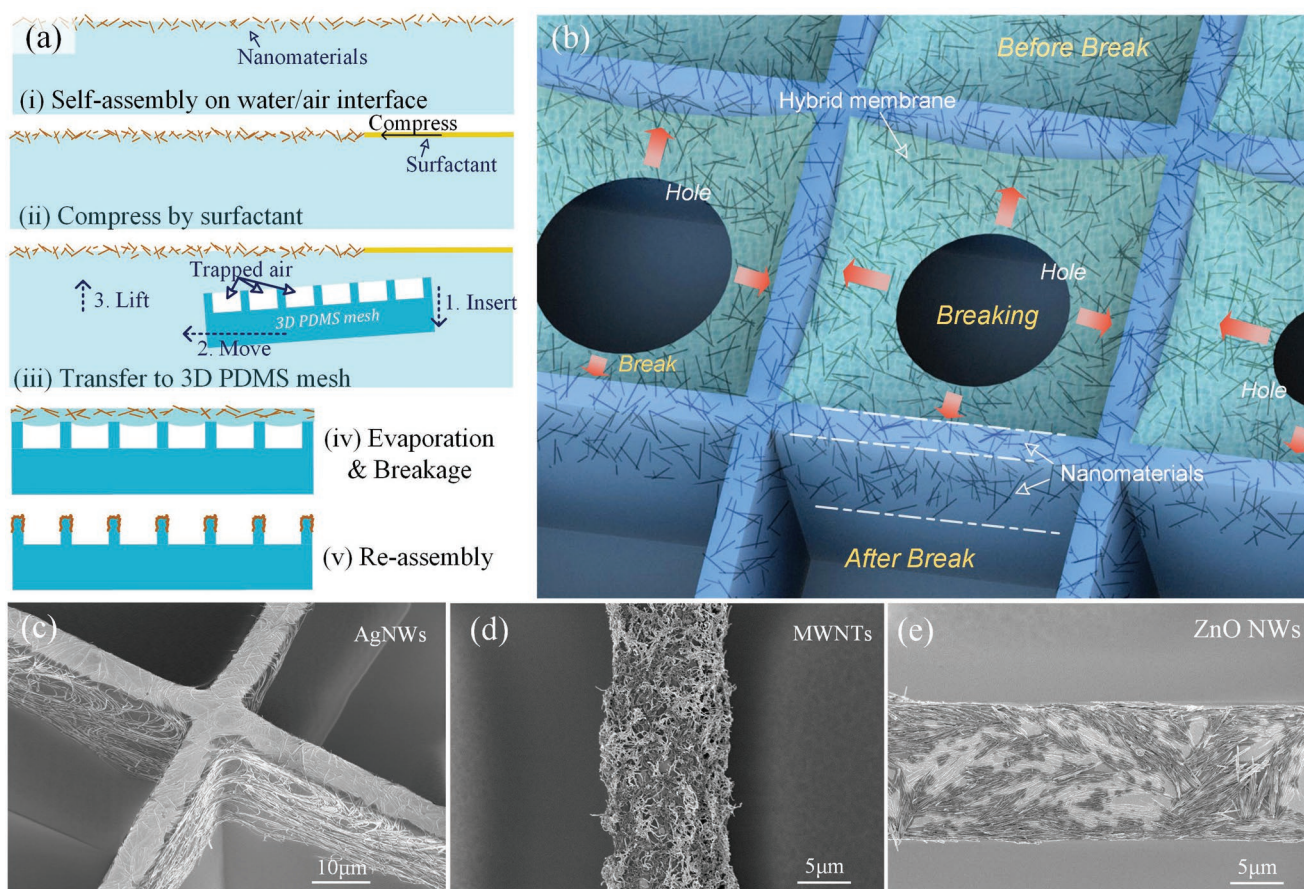


Figure 1. Schematic diagram of fabrication process and SEM images of 3D nanomaterial grids. a) Fabrication process including five main steps: i) Nanomaterials are introduced onto water/air interface by gentle injection of suspension. ii) Surfactant is added to compress the network of nanomaterials for easier transfer. iii) The elastomer with microstructures is immersed into water, and moved to be underneath the network of nanomaterials and then slowly lifted up to transfer hybrid membrane made of water and nanomaterials. Note that no water permeates into microstructures due to the trapped air inside. iv) Solvent evaporates continuously and later the hybrid membrane breaks and shrink toward the edges of supporting microstructures. v) Nanomaterials reassemble along the microstructured patterns. b) Illustration of breakage process of hybrid membrane on microwells during solvent evaporation, indicating the accumulation of nanomaterials to the top and sidewall of microstructures under the liquid shrinking force. The status before, during, and after breakage are marked. c) SEM image of AgNWs (30° tilt) covered only on top surface and sidewalls of PDMS microwalls. d, e) SEM images of MWCNTs and ZnO NWs assembled on PDMS microwalls by the same method, respectively (top view).

Researchers also succeeded in fabrication of high-aspect-ratio nanogrid structure that has a sheet resistance of $15.2 \, \Omega \, \text{sq}^{-1}$ and an optical transmittance of 85.4% via capillary assembly of Ag nanoparticles.^[12a]

Herein, we present a novel fabrication strategy of 3D deposition to introduce transparency for various nanomaterial networks by exploiting the breakage phenomenon of self-assembled nanomaterial–water membrane on designed polydimethylsiloxane (PDMS) microwalls. When the liquid film breaks on 3D microstructures due to the drying process, the nanomaterial sheet adheres effectively onto both the top surface and the sidewalls of the microstructures and thus allows for higher transparency while preserving the nanomaterial mass. Silver nanowires (AgNWs), carbon nanotubes (CNTs), zinc oxide nanowires (ZnO NWs), and silica sphere are demonstrated in this paper for successful attachment onto microstructures. Because of little waste of nanomaterials by this fabrication strategy, nanomaterial networks such as AgNW networks are highly transparent, remarkably conductive, and

environmentally friendly. It has a very low resistance of less than $100 \, \Omega \, \text{sq}^{-1}$ for high transmittance of larger than 85%. The liquid film breakage phenomenon during evaporation has been carefully investigated to optimize the 3D mesh design and also to design a simple and reliable fabrication process that is scalable. This proposed method can possibly pave the way for future transparent stretchable devices by layer-by-layer technique with various nanomaterials, with a cost-efficient and waste-reducing method.

2. Results and Discussion

2.1. Fabrication Process

The methodology is mainly based on Langmuir–Blodgett (LB) method,^[15] which is the common fabrication method for thin-layer nanomaterial deposition. The strategic steps of the proposed method are shown in **Figure 1a**. Briefly, nanomaterial

suspension is first introduced onto deionized (DI) water and air interface to form the nanomaterials–water membrane. Nanomaterials float on water surface and self-assemble together as a network. After nanomaterials have occupied most of the water surface, manual injection stops and is followed by one compression process using a specific surfactant, which enhances the mechanical strength of hybrid membrane.

PDMS substrate with microstructures is prepared by transferring microstructures from prefabricated silicon molds. It is first immersed into water, then moved into position under the nanomaterial network floating on the surface of the water and then lifted gently to transfer them to the elastomer surface. The air in PDMS microstructures is trapped because of the weak wettability between PDMS and water. The hybrid membrane is then supported by microwalls during its evaporation process. It can sustain the entire membrane until the breakage phenomenon happens. The phenomenon is illustrated in detail by schematic diagram in Figure 1b. Finally, the nanomaterials can reassemble onto microstructures of PDMS substrate. The experiments were carried out at room temperature and relative humidity of 40–60%. The assembly process took few minutes. See the Experimental Section for detailed information.

In conventional LB method, the hybrid membrane can be ideally transferred onto flat substrates, e.g., glass slide, silicon slide, PDMS, etc. As described above, our fabrication method also utilizes the hybrid membrane on water/air interface as a base element, but with a microstructured substrate shown in Figure 1b, which has large and deep square holes with thin boundaries. Herein, the description of the space surrounded by microwalls is named as “microwell”, of which the period is defined as p , the width and depth is called as w and d , respectively. Unlike the conventional LB method with hydrophilic substrate surface for uniform nanomaterial attachment,^[16] this fabrication strategy needs no pretreatment of the microstructured substrate. In contrast, the hydrophobicity of elastomer (e.g., PDMS) is quite important to preserve the trapped air in microstructures. No leakage of air in the microwells is expected for the floating hybrid membrane, which can be considered as the liquid lid of the microwell array during the process.

Water evaporation happens continuously after hybrid membrane transfer and causes membrane breakage eventually. Figure 1b shows the status before, during, and after the breakage. At the top of the microwell, the hybrid membrane appears as a concave structure by resultant forces of surface tension, interfacial forces, and gravity. During membrane rupture, nanomaterials advance onto the sidewalls of microstructures. After complete water evaporation, nanomaterials remain on top surface and top part of sidewalls as shown in bottom microwell.

The observation of sample by scanning electron microscope (SEM) in Figure 1c can proof the described process. The image with 30° of tilt shows clear distribution of AgNWs, which verifies their existence only on the top surface and top part of sidewalls. The nanowires on sidewall are not randomly oriented. A clear orientation parallel to top surface can be observed, which in turn verifies the shrinkage process during hybrid membrane breakage. The fabrication strategy can also be used for other nanomaterials. Figure 1d,e shows SEM images of multi-walled CNTs (MWCNTs) and ZnO NWs on top surface of microwalls, respectively.

Although the parameters for them are quite different, the basic mechanism is the same for various nanomaterials.

2.2. Hybrid Membrane Breakage

The evaporation of water, which was recorded and shown in Figure 2a–f by optical microscopy, leads to the decrease of membrane thickness. The time before breakage is determined by self-assembly parameters, species of nanomaterials, and the transfer method. During the process, hybrid membrane in each microwell reaches its critical thickness and breaks one after the other. The direction of breakage depends on the thickness gradient of the hybrid membrane after the transfer process. Using the marked microwell for close observation, hybrid membranes connect together as an unbroken membrane on the top surface in Figure 2a,b. The microwalls isolate membrane rupture as shown in Figure 2c,d. The surrounding hybrid membranes break afterward and the breaking process speeds up in Figure 2e. The last unbroken membrane cannot sustain its stability and collapses eventually in Figure 2f. The inserted image in Figure 2a shows the contact angle (CA) of dilute water droplet (3 μ L) on PDMS with microstructure ($w = 5 \mu\text{m}$, $p = 100 \mu\text{m}$, w_5_p100), indicating high hydrophobicity of PDMS microstructures.^[17]

To further analyze the breakage process, a high-speed camera captured images every 0.625 ms (shown in Figure 2g). The middle microwell has the unbroken membrane and its left and right ones have already collapsed. From the first image at 0 ms, a tiny hole in the center can be observed. Its size increases gradually from 0 to 1.875 ms and it suddenly breaks during 1.875–2.5 ms. In the image at 2.5 ms, AgNWs are pulled by liquid flow to sidewalls of microwell. Afterward, the water gradually evaporates with time and AgNWs reside on the top surface and sidewalls of microstructures.

2.3. Characterization of Nanomaterial Grids

With the surface modification of AgNWs, concentration adjustments, and evaporation control, the breakage process can be tailored in a large scale. In our experiments, transparent samples over $2 \times 3 \text{ cm}^2$ can be obtained successfully. Figure 3a shows a sample with perfect nanomaterial grids over $2.8 \times 4 \text{ mm}^2$. The photo was taken by dark-field optical microscopy, in which the unscattered light is excluded from the image resulting in very dark image and highlight of nanowire boundaries. The inserted image illustrates more detailed information of connections between nanowires. The LB method is regarded as one effective method of monolayer nanomaterials fabrication. By using the microwells as the supporting substrate in the LB method, monolayer AgNWs can be observed as shown in Figure 3a. Besides, the AgNWs on the top surface of a microwell are analyzed by atomic force microscope (AFM). Figure 3b illustrates the 3D reconstruction by scanning data of AFM, in which the substrate with a monolayer of AgNW is shown. The substrate is not flat because it was transferred from dry-etched silicon wafer. The height information of red and blue lines in Figure 3b is shown in Figure 3c, in which the diameter of AgNWs are 59.6 and 43.0 nm, respectively.

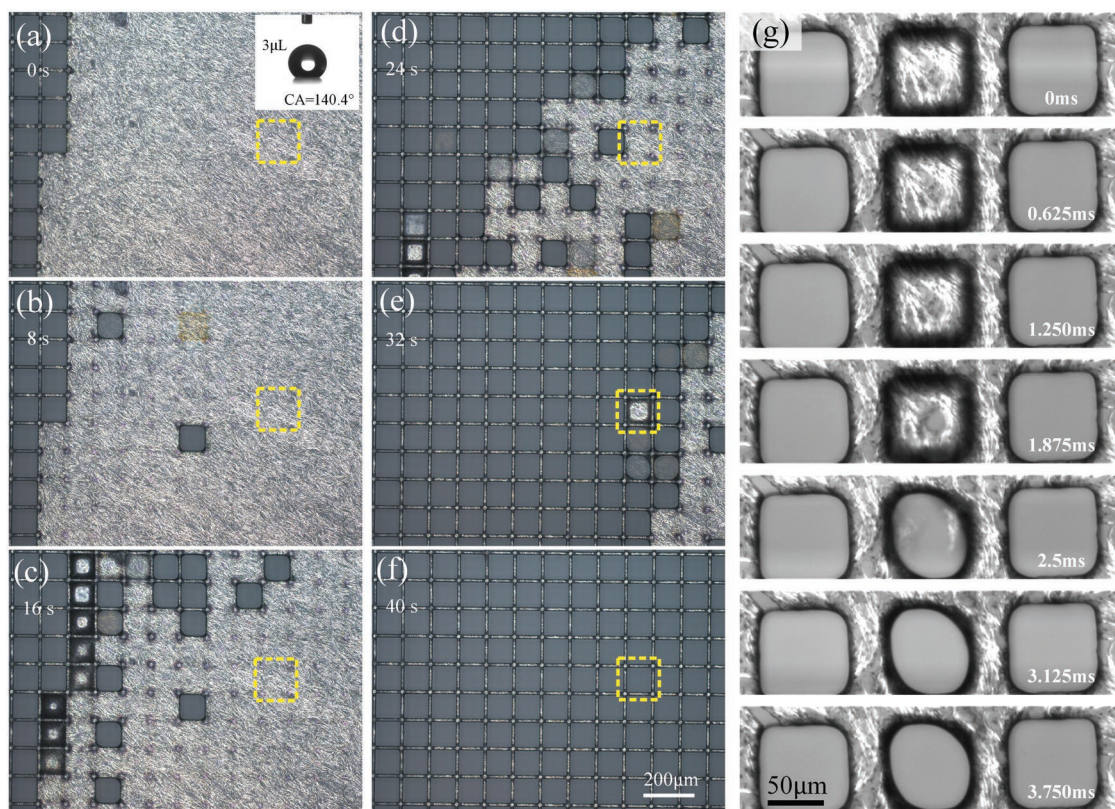


Figure 2. Breakage process of AgNWs/water membrane. a–f) After process steps of Figure 1a,i–iii, AgNWs/water membrane is suspended atop and supported by microstructures with the supporting of trapped air. As evaporation increases over time, the mechanical integrity becomes weaker. When it is too weak to support the suspension of the composite membrane, breakage occurs. The breakage process happens and spreads to neighboring microwells. The images were taken every 8 s. The inserted image in (a) shows the CA of water and microstructured PDMS (w5_p100, CA = 140.4°), illustrating the weak wettability. g) High-speed-camera recorded the breakage process of a single membrane every 0.625 ms. From 0 to 1.875 ms, the hole in the center clearly increases its size and breaks at next period. At 2.5 ms, AgNWs were pulled toward the sidewall of microstructure and the water evaporated continuously. It is worth mentioning that the AgNWs/water membrane is slightly under the top surface of PDMS because of combined effect of surface tension, gravity, and interfacial forces.

The cross-section view of the nanowire microgrid is shown in Figure S4 (Supporting information). The optical image focuses on the deeper layer of the microstructure and gives a clear idea of the nanowires distribution. In the boundary of flat and structured PDMS surfaces shown in Figure 3d, the network connects together, however, a clear surface proportion difference of AgNWs can be observed. For other kinds of surface microstructures, e.g., hexagon holes, serpentine networks, and honeycomb meshes in Figure 3e–g, the same fabrication flow can also work. This progress can make this fabrication suitable for many different surface microstructures in various applications. The detailed analysis of the breakage phenomenon is given in Discussion in the Supporting Information, which includes the discussion of two critical points for the process, as well as the geometrical parameters for successful hybrid membrane breakage.

2.4. Light Transmittance Test

For conventional network on flat surface, higher surface density leads to lower light transmittance and vice versa. By distributing nanomaterials onto microwells, this fabrication strategy

obtains nanomaterial networks with both high density and high transparency.

We fabricated different samples with multiple deposition times on flat and microstructured surfaces. **Figure 4a** shows the samples with one, two, four, and eight layers on colored printing paper. The microstructured samples have higher transmittance even with eight layers. However, the flat surface has obvious transparency change with more deposition layers. The SEM images in Figure 4b show complete surface occupation of flat samples with large light transmittance space for microstructure ones. With one-time deposition, AgNWs do not occupy the top surface of microwells completely. The surface occupation ratio as well as the thickness increases with the deposition times.

The results of transmittance test of these samples, shown in Figure 4c, match with the optical images in Figure 4a. The light over the wavelength ranging from 400 to 800 nm was used for this test. The samples with the same layer(s) of AgNWs on flat surfaces were tested as the control group. With more area for light transmission, the AgNW grids are more transparent than flat ones. Even the AgNW grids with eight-time deposition transmit more light than the flat one with one-time deposition.

The resistance does not go higher by this kind of deposition strategy. In contrast, the conductance becomes better. The

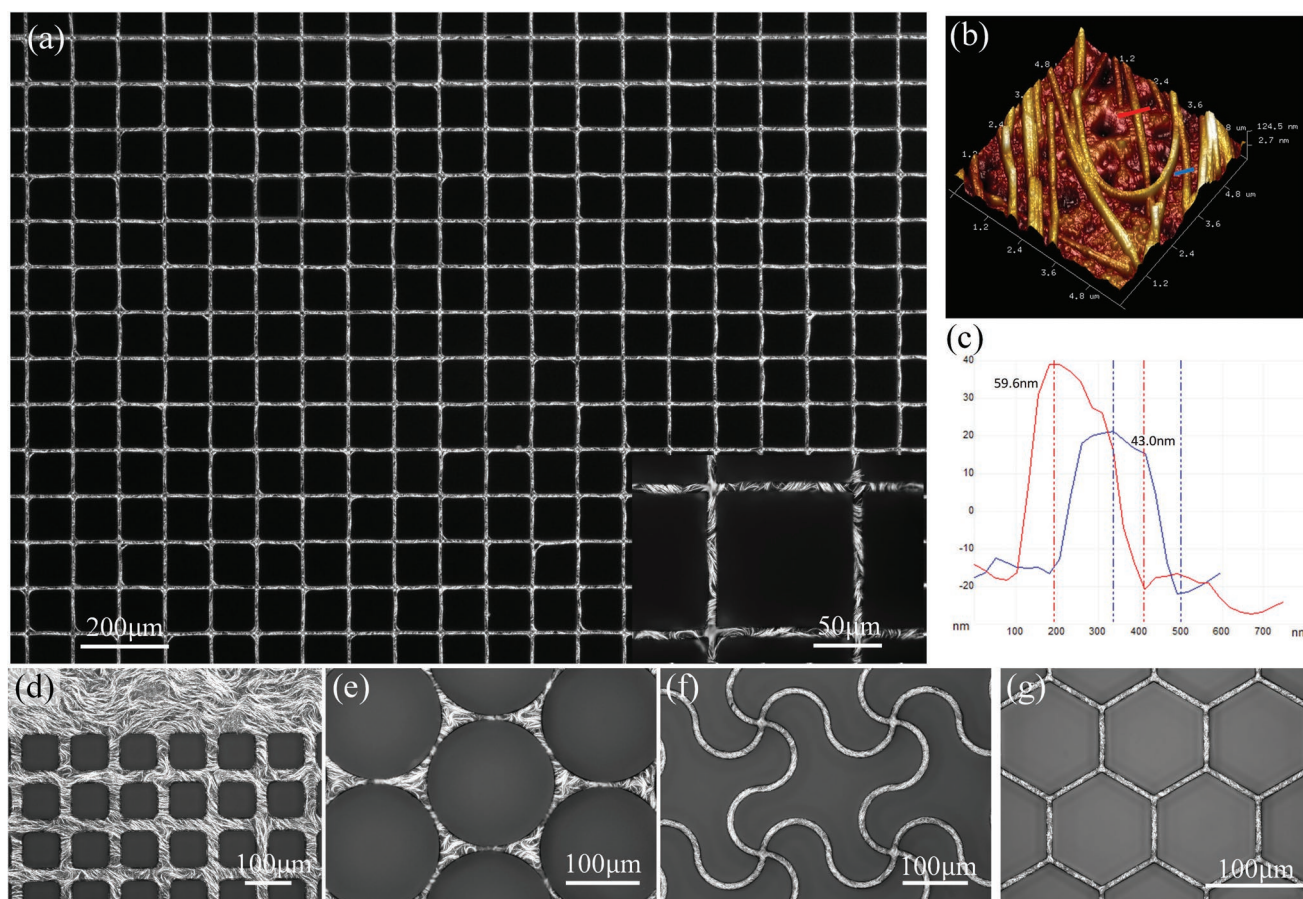


Figure 3. Characterization of AgNWs on the top surface of microwalls. a) Dark-field optical-microscope image of AgNWs on microwalls in large scale (w5_p100). The inserted image is in high magnification. b, c) Surface roughness test of AgNWs on PDMS by AFM (average roughness = 27.1 nm). The diameter of nanowire is around 50 nm. d) SEM image of AgNWs on a flat surface and on the boundary of microstructured PDMS (w25_p100), indicating the remarkable coverage of this fabrication technique. Moreover, compared with the flat nanowire networks, the patterned nanowire networks possess a better light transmission feature while keeping a similar conductive capability. e–g) Three different structures, including hexagon holes, serpentine networks, and honeycomb meshes, were introduced to demonstrate the universality of this fabrication approach.

specular transmittance versus sheet resistance for the two cases is plotted in Figure 4d, which shows the resistance decrease for microgrids compared with flat ones. There are two reasons. First, the conductive nanomaterials in microgrids are not less than that on a flat surface, because the nanowires on sidewalls connect to the top surface. Second, the connection of nanowires is better with each other on sidewalls. The nanowire monolayer transferred from the water/air interface forms a monolayer and leads to weak interconnection, which explains the high sheet resistance of AgNW monolayers (see Figure 4d). The nanowires on sidewalls, however, have higher possibility for random interconnections after reassembly process in liquid breakage.

With the increase of deposition times for each case, the sheet resistance drops dramatically from hundreds of ohms to several ohms because of greatly increased nanowire connection between layers. For instance, the microgrid sample with four layers of deposition has a sheet resistance of $6.98 \Omega \text{ sq}^{-1}$ and an optical transmittance of 83.83%. The microgrid can also function under stretching, especially when it has a serpentine design to release stress. The resistance change during stretch and release was tested under 50% elongation. The result in

Figure S8 in the Supporting Information reveals a moderate and stable resistive change during stretching in long-term test.

3. Conclusion

In this paper, we present a novel fabrication strategy for scalable transparent nanomaterial microgrids. Thanks to the liquid film breakage phenomena and process, this strategy offers a new way to distribute nanomaterials to sidewalls of microstructures to gain more space for light transmittance. The liquid behavior before, during, and after breakage was analyzed by close observation with multiple methods. By parametric study, the ideal conditions for nanomaterial microgrids, as well as several failure tests, have been proposed. With only minute waste of nanomaterials for conductance, AgNW grids exhibit low resistance and high transparency as well. Additionally, various nanomaterials have been demonstrated to assemble onto microstructures for multilayers, which indicates promising applications by various nanomaterials on different layers for transparent and functional devices.

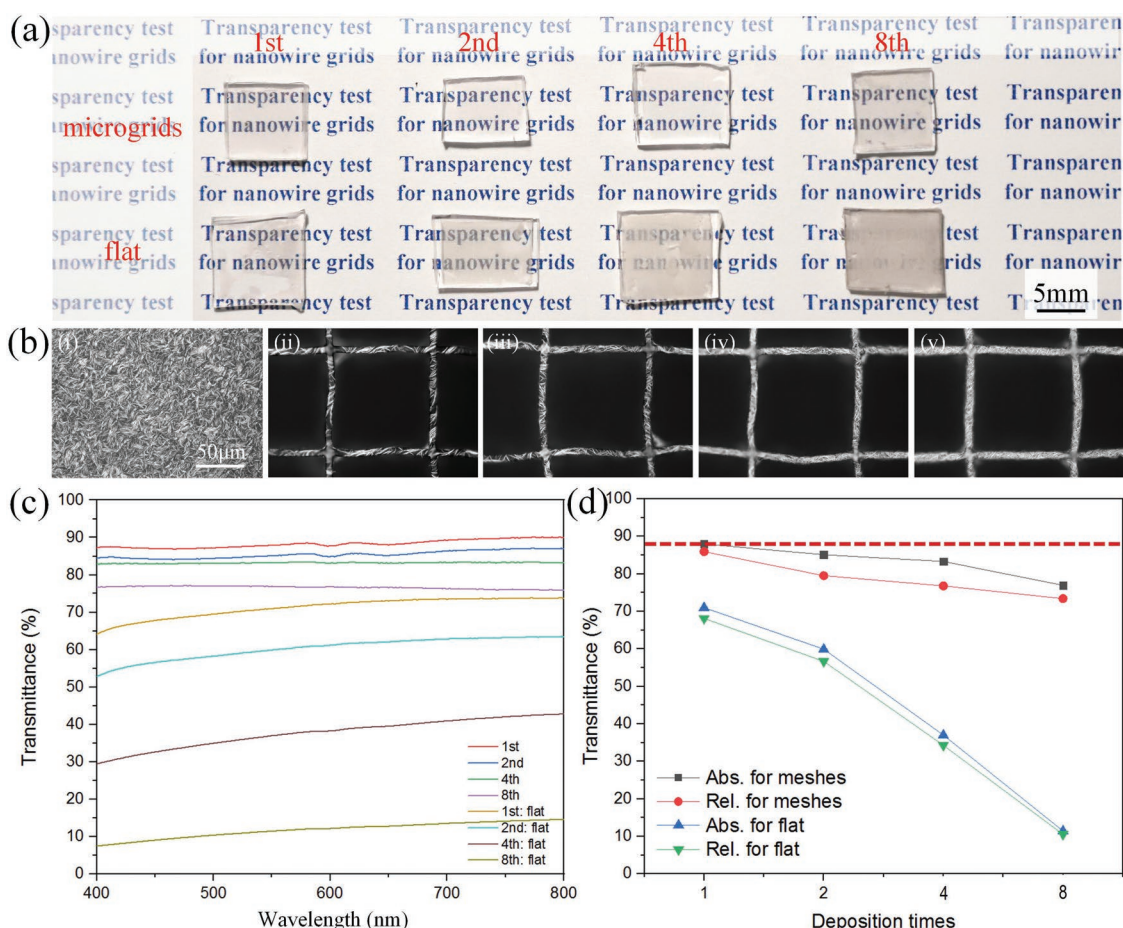


Figure 4. Characterization of optical transmission for AgNWs networks on various substrates. AgNWs deposited on flat and structured PDMS (w5_p100). Repeated deposition by the same parameters for one time, two times, four times, and eight times. a) Optical images of PDMS samples. b) (i–v) are their microscope images respectively. c) Transmission results for different surfaces with first, second, fourth, and eighth deposition times. Note that the optical transmission results are obtained without considering the substrates. d) Plot of specular transmittance versus sheet resistance at wavelength of 550 nm for AgNWs on flat surface and microwalls.

4. Experimental Section

Silicon Molds and Structure Transfer: Silicon molds were prepared by deep reactive ion etching and followed by an antiadhesion layer deposition. A 2 μm positive photoresist (AZ 9221) was first deposited on silicon wafer and followed by photolithography with critical dimension of 2 μm (exposure dose: 175 mJ cm^{-2}). The wafer was then dry etched to 40–60 μm by the Bosch process. After the removal of photoresist by oxygen plasma stripper, a 50 nm parylene coating was deposited as an antiadhesion layer by chemical vapor deposition.^[18] PDMS was used to transfer the microstructures from silicon molds in following steps: First, PDMS elastomer and cross-linker (Sylgard184, Dow Corning) were thoroughly mixed in a 10:1 ratio w/w, poured onto silicon molds (8 g 4 in.⁻¹ wafer), and then kept on an optical table for self-leveling and degassing in a low-pressure chamber for 30 min. After polymerization at 100 °C for 30 min, PDMS membrane was peeled off gently from the molds to ensure successful transfer. The image of silicon mold before and after transfer and the transferred PDMS with microstructures can be referred in Figures S1 and S2 in the Supporting Information, respectively.

Self-Assembly of AgNWs: AgNWs in isopropyl alcohol (IPA) (0.5 mg mL^{-1}) were first diluted to 0.1 mg mL^{-1} and then treated by 1-octadecanethiol (0.1 $\times 10^{-3}$ M in IPA) with the same volume for 12 h. Thiol was easily self-assembled onto the surface of AgNWs^[15b] to increase the hydrophobicity of nanowires and assisted them onto to

form a water/air interface. The mixed solution was then diluted to 1/8, 1/16, 1/24, and 1/32. An appropriate amount of DI water was prepared in the container for the self-assembly process. The diluted suspension was then injected at low velocity until nanowires occupied liquid surface completely to form the water/air interface. Sodium dodecyl sulfate (1 mg mL^{-1}) was used as the surfactant to slightly compress the nanowire network for easy transfer. The samples were inserted into the water and then lifted up to the transfer hybrid membrane to microwells. The self-assembled AgNWs network floating on water surface is shown in Figure S3 in the Supporting Information.

Self-Assembly of Other Nanomaterials: MWCNTs, ZnO, and graphene oxide were first dispersed in IPA (1 mg mL^{-1}) and treated by ultrasound for 3 h, 15, and 15 min, respectively. The suspensions were then diluted to 1/20 and injected by syringe pump without any surface treatment to form the water/air interface. These three kinds of nanomaterials could easily stay on the surface of the solution. Other steps were similar to the ones for AgNWs. For multilayer nanomaterial grids, the layer-by-layer technique was applied. After drying the sample with nanomaterials at 60 °C for 30 min, it was used as a substrate for nanomaterial transfer as the next layer. Figure S7 in the Supporting Information gives several examples by using this method, including AgNWs/ZnO NWs, AgNWs/silica microspheres, and AgNWs/MWCNTs hybrid networks.

Characterization: SEM images were characterized using an SEM LEO 1550 operated at 1 kV beam voltage. The sheet resistances of AgNW grids samples were carried out by four-probe method using a linear

arrayed four-point head. Before the resistance test, thermal treatment at 150 °C for 20 min was needed to remove thiols on the surface of AgNWs. Figure S6 in the Supporting Information gives the resistance change during designed thermal treatment process. The optical images were taken by optical microscope (Digital Sight, Nikon) and high-speed camera (1600 fps). The light transmittance was tested by CARY 5 UV-vis–near-infrared spectrophotometer. For the surface roughness, AFM (FastScan, Bruker) was applied at contact mode for high resolution.

Supporting Information

Supporting Information is available from the Wiley Online Library or from the author.

Acknowledgements

The authors thank Dr. Christopher Tse from École Polytechnique Fédérale de Lausanne for polishing language. This work was supported by State Scholarship Fund from China Scholarship Council (no. 201706010247), National Key R&D Project from Minister of Science and Technology, China (2018YFA0108100 and 2016YFA0202701), the National Natural Science Foundation of China (grant nos. 61674004, 61176103, 61804023), and Key R&D Program of Sichuan Province (no. 2018GZ0527).

Conflict of Interest

The authors declare no conflict of interest.

Keywords

3D microstructure, liquid breakage, self-assembly, transparent device

Received: May 14, 2019

Revised: June 22, 2019

Published online: August 15, 2019

- [1] J. Lee, P. Lee, H. B. Lee, S. Hong, I. Lee, J. Yeo, S. S. Lee, T. S. Kim, D. Lee, S. H. Ko, *Adv. Funct. Mater.* **2013**, 23, 4171.
- [2] a) I. E. Stewart, A. R. Rathmell, L. Yan, S. Ye, P. F. Flowers, W. You, B. J. Wiley, *Nanoscale* **2014**, 6, 5980; b) C. Sachse, N. Weiß, N. Gaponik, L. Müller-Meskamp, A. Eychmüller, K. Leo, *Adv. Energy Mater.* **2014**, 4, 1300737.
- [3] a) D. S. Hecht, L. Hu, G. Irvin, *Adv. Mater.* **2011**, 23, 1482; b) S. Ye, A. R. Rathmell, Z. Chen, I. E. Stewart, B. J. Wiley, *Adv. Mater.* **2014**, 26, 6670.
- [4] a) A. Chiolerio, S. Bocchini, F. Scaravaggi, S. Porro, D. Perrone, D. Beretta, M. Caironi, C. F. Pirri, *Semicond. Sci. Technol.* **2015**, 30, 104001; b) F. C. Krebs, S. A. Gevorgyan, J. Alstrup, *J. Mater. Chem.* **2009**, 19, 5442; c) S. I. Na, S. S. Kim, J. Jo, D. Y. Kim, *Adv. Mater.* **2008**, 20, 4061.
- [5] a) W.-K. Kim, S. Lee, D. H. Lee, I. H. Park, J. S. Bae, T. W. Lee, J.-Y. Kim, J. H. Park, Y. C. Cho, C. R. Cho, *Sci. Rep.* **2015**, 5, 10715; b) J. Zou, H.-L. Yip, S. K. Hau, A. K.-Y. Jen, *Appl. Phys. Lett.* **2010**, 96, 96; c) D. Ghosh, T. Chen, V. Pruneri, *Appl. Phys. Lett.* **2010**, 96, 041109.
- [6] C. Pan, K. Kumar, J. Li, E. J. Markvicka, P. R. Herman, C. Majidi, *Adv. Mater.* **2018**, 30, 1706937.
- [7] a) Y. Kim, J. Zhu, B. Yeom, M. Di Prima, X. Su, J.-G. Kim, S. J. Yoo, C. Uher, N. A. Kotov, *Nature* **2013**, 500, 59; b) M. Sangermano, A. Chiolerio, G. Marti, P. Martino, *Macromol. Mater. Eng.* **2013**, 298, 607.
- [8] D. Langley, G. Giusti, C. Mayousse, C. Celle, D. Bellet, J.-P. Simonato, *Nanotechnology* **2013**, 24, 452001.
- [9] a) N. Liu, A. Chortos, T. Lei, L. Jin, T. R. Kim, W.-G. Bae, C. Zhu, S. Wang, R. Pfattner, X. Chen, *Sci. Adv.* **2017**, 3, e1700159; b) S. H. Chae, W. J. Yu, J. J. Bae, D. L. Duong, D. Perello, H. Y. Jeong, Q. H. Ta, T. H. Ly, Q. A. Vu, M. Yun, *Nat. Mater.* **2013**, 12, 403.
- [10] M. Song, D. S. You, K. Lim, S. Park, S. Jung, C. S. Kim, D. H. Kim, D. G. Kim, J. K. Kim, J. Park, *Adv. Funct. Mater.* **2013**, 23, 4177.
- [11] S. Han, M. K. Kim, B. Wang, D. S. Wie, S. Wang, C. H. Lee, *Adv. Mater.* **2016**, 28, 10257.
- [12] a) J. Kang, C.-G. Park, S.-H. Lee, C. Cho, D.-G. Choi, J.-Y. Lee, *Nanoscale* **2016**, 8, 11217; b) S. De, T. M. Higgins, P. E. Lyons, E. M. Doherty, P. N. Nirmalraj, W. J. Blau, J. J. Boland, J. N. Coleman, *ACS Nano* **2009**, 3, 1767.
- [13] a) D. J. Lipomi, M. Vosgueritchian, B. C. Tee, S. L. Hellstrom, J. A. Lee, C. H. Fox, Z. Bao, *Nat. Nanotechnol.* **2011**, 6, 788; b) Y. Zhu, F. Xu, *Adv. Mater.* **2012**, 24, 1073.
- [14] K. MináCho, M. LiangáJin, C. JináAn, S. HwanáKo, *Nanoscale* **2016**, 8, 14257.
- [15] a) K. Ariga, Y. Yamauchi, T. Mori, J. P. Hill, *Adv. Mater.* **2013**, 25, 6477; b) A. Tao, F. Kim, C. Hess, J. Goldberger, R. He, Y. Sun, Y. Xia, P. Yang, *Nano Lett.* **2003**, 3, 1229; c) M. Szekeres, O. Kamalin, R. A. Schoonheydt, K. Wostyn, K. Clays, A. Persoons, I. Dékány, *J. Mater. Chem.* **2002**, 12, 3268.
- [16] T. Szabó, V. Hornok, R. A. Schoonheydt, I. Dékány, *Carbon* **2010**, 48, 1676.
- [17] a) T. L. Liu, Z. Chen, C.-J. Kim, *Soft Matter* **2015**, 11, 1589; b) P. Tsai, R. G. Lammertink, M. Wessling, D. Lohse, *Phys. Rev. Lett.* **2010**, 104, 116102.
- [18] Y. Chen, W. Pei, R. Tang, S. Chen, H. Chen, *Sens. Actuators, A* **2013**, 189, 143.